Solitary wave characteristics on the fine structure of mesospheric sporadic sodium layer

Shican Qiu[1,2]*, Mengxi Shi[1], Willie Soon[3,4], Mingjiao Jia[5], Xianghui Xue[2,6], Tao Li[2,6], Peng Ju[1], Xiankang Dou[2,6]*

5   [1] Department of Geophysics, College of the Geology Engineering and Geomatics, Chang'an University, Xi'an, 710054, China.

[2] Key Laboratory of Geospace Environment, Chinese Academy of Sciences, University of Science & Technology of China, Hefei, Anhui, 230026, China

[3] Center for Environmental Research and Earth Sciences (CERES), Salem, MA 01970, USA

10 [4] Institute of Earth Physics and Space Science (ELKH EPSS), 9400, Sopron, Hungary.

[5] Shandong Guoyao Quantum Lidar Co., Ltd., Jinan, 250101, China.

[6] Mengcheng National Geophysical Observatory, School of Earth and Space Sciences, University of Science and Technology of China, Hefei, Anhui, 230026, China.

Correspondence to: Shican Qiu (*scq@ustc.edu.cn*) and Xiankang Dou (*dou@ustc.edu.cn*)

15 **Abstract.** The most fantastic phenomenon of the mesospheric sodium layer is the so-called sporadic sodium layer (SSL or Na_S), which are proposed to be closely related to wave fluctuations. Solitary wave is a particular solution of partial differential equation whose energy travels as a localized wave packet, and a soliton is a special solitary wave which has a particle-like behavior with strong stable form. In this research, the solitary wave theory is applied for the first time to study the fine structure of Na_S. We perform soliton fitting processes on the observed data from the Andes Lidar Observatory, and

20 find out that 24/27 Na_S events exhibit similar features/characteristics to a soliton. Time series of the net anomaly of the Na_S reveal the same variation process to the solution of a generalized five-order KdV equation. Our results therefore suggest the Na_S phenomenon would be an appropriate tracer for nonlinear wave studies in the atmosphere.

Keywords: sporadic sodium layers, solitary waves, soliton, lidar

25

1 Introduction

The sodium layer locates at about 80–110 km above, normally with a Gaussian distribution formed through the ablation of meteors (Kane and Gardner, 1993; Kopp, 1997). The most fantastic phenomena of the sodium layer is the so-called sporadic sodium layer (SSL or Na_S) (Cox et al., 1993; Gardner et al., 1993; Mathews et al., 1993). For the Na_S event, the sodium

5 density will increase rapidly and could be more than double the background value (e.g. with an intensity factor >2) within several minutes in a narrow altitude range (Hansen and von Zahn, 1990). Na_S last from tens of minutes to several hours (Nagasawa and Abo, 1995; Prasanth et al., 2007), and their full width at half maximum (FWHM) usually less than 5 km or sometimes only 1–2 km (Hansen and von Zahn, 1990; Nagasawa and Abo, 1995; Prasanth et al., 2007). Since first reported on 1978 (Clemesha et al., 1978), a lot of mechanisms have been proposed (Cox et al., 1993; von Zahn et al., 1987; Zhou et

10 al., 1993). The current evidences conform the ion-molecule theory is the most possible mechanism for Na_S, based on the local observation (Dou et al., 2009; Dou et al., 2010; Hansen and von Zahn, 1990; Heinrich et al., 2008; Heinselman et al., 1998; Kirkwood and Nilsson, 2000; Nesse et al., 2008; Qiu et al., 2016; von Zahn and Hansen, 1988; Williams et al., 2006), and model simulation (Collins et al., 2002; Cox et al., 1993; Cox and Plane, 1998; Plane et al., 2015; Plane, 2003). The sodium ions from E_S could probably provide sufficient neutral sodium atom source through recombination with free

15 electrons (Collins et al., 2002; Cox et al., 1993; Cox and Plane, 1998; Plane et al., 2015; Plane, 2003; Qiu et al., 2020).

On the other hand, mesospheric sodium layer observations by lidars are believed to be a tracer to possibly identify the atmospheric wave signals (Gardner and Voelz, 1987; Gardner et al., 2019; Gong et al., 2015; Li et al., 2007a; Li et al., 2007b; Xu and Smith, 2004). The current existing mechanisms indicate that Na_S is closely related to wave fluctuations (Clemesha et al., 1997; Kane et al., 1991; Qian et al., 1998; Zhou et al., 1993; Zhou and Mathews, 1995). Many observational results

20 reveal Na_S often occur accompanied by gravity waves (Ban et al., 2015; Li et al., 2007a; Li et al., 2007b; Qian et al., 1998). Meanwhile, the fine structures of Na_S exhibit distinct characters related to waves on small time scale (Chen and Yi, 2011; Liu and Yi, 2009; Liu et al., 2013). The bursts of the sodium atoms show a pulse period of 30 seconds (Liu and Yi, 2009), indicating a wave fluctuation effect on the evolution of Na_S.

Recently, a peculiar kind of the nonlinear waves, which is called the solitary wave, has been widely studied (Belashov

25 and Vladimirov, 2005; Benci and Fortunato, 2014; Wazwaz, 2009). It was first reported by John Scott Russell (1808–1882), when he was observing the motion of a boat rapidly drawn along a narrow channel (Russell, 1844). From then on, many researchers have made a lot of studies on the theoretical derivation and exploration on this nonlinear problem. Generally speaking, the solitary wave is a particular solution of partial differential equation whose energy travels as a localized wave packet, and a soliton is a special solitary wave which has a particle-like behavior with strong stable form (Benci and

30 Fortunato, 2014). Soliton is of great interest to the modern physics and mathematics (Belashov and Vladimirov, 2005; Benci and Fortunato, 2014; Wazwaz, 2009). It is a fundamental wave structure for the nonlinear wave processes, which plays an important role in the wide spectrum of areas of research related to the wave physics, e.g., in hydrodynamics, plasma physics, condensed matter, and optics (Belashov and Vladimirov, 2005). The solitary waves nowadays are widely applied for the

Atmospheric
Chemistry
and Physics
Discussions

Earth science especially involving ocean and atmosphere, such as surface waves, ion-acoustic waves, magnetosonic waves, internal gravity waves, Raleigh waves off a seismic source, and so on (Belashov and Vladimirov, 2005).

The nonlinear solitary wave theory was first decisively exerted by Korteweg and de Vries as the simplified model equation for surface waves on shallow water,

$$\frac{\partial u}{\partial t} + \alpha u \frac{\partial u}{\partial x} + \beta \frac{\partial^3 u}{\partial x^3} = 0, \tag{1}$$

5

with solutions of stable solitary waves [*Korteweg and Vries*, 1895](Korteweg and Vries, 1895). The term soliton was first introduced in 1965 by Zabusky and Kruskal who demonstrated that the Korteweg-de Vries equation (KdV equation) reveals hidden linear properties, allowing a solution in the form of a nonlinear solitary wave propagating without changing its profile (Zabusky and Kruskal, 1965). These authors also pointed out that the soliton has two important properties: (1) extremely
10   stable wave packet like a particle; (2) invariant even under particle collisions (Zabusky and Kruskal, 1965).

In this research, the solitary wave theory has been deduced and compared with the lidar observations. We perform particular data processing on the observed results from a narrow band lidar at the Andes Lidar Observatory (Liu et al., 2016). We find that the fine structure of Na_S evolutions exhibit similar characters to a soliton, indicating a common existence of solitary waves on the mesopause region. The evolution of the net anomaly of the Na_S peak profiles exhibit the same
15   characters to the solution of five-order KdV equation. Our results therefore suggest the Na_S phenomenon would be a possible tracer for nonlinear wave studies.

2 The solitary wave theory and data processing

2.1 The nonlinear and dispersion effects

Consider a one-dimensional wave at the moment t, the particle number density at x in the medium is given by $n(x, t)$. Under
20   the conservation of particle number, there is

$$\frac{dn}{dt} = 0, \tag{2}$$

where *n* could possibly be regarded as the input of sodium sources from Na^+ through chemical reactions. After the input, $n(x, t)$ would possibly undergo the evolution ways: the convergence or divergence.

The full derivative form for $n(x, t)$ can be expanded as

25

$$\frac{\partial n}{\partial t} + v \frac{\partial n}{\partial x} = 0, \tag{3}$$

where $\frac{dx}{dt} = v$ is the velocity of the particle movement. This equation has a generalized solution:

$$n(x, t) = f(x - v(n)t). \tag{4}$$

This solution indicates each part of the wave has a different speed of $v(n)$. When $\frac{dv}{dn} > 0$, $v(n)$ would increase with increasing density n. Therefore the wave packet front becomes steeper and steeper as the wave propagates, leading to a
30   nonlinear effect of convergence (Fig. 1a).

On the other hand, a wave propagating in x direction can be expressed as

$$u(x, t) = A\exp[i(kx - \omega t)], \qquad (5)$$

where u is the wave function, A is the amplitude, k is the wave number, and ω is the angular frequency. The phase velocity v_p and group velocity v_g are given by,

$$v_p = \frac{\omega}{k}, \qquad (6)$$

and

$$v_g = \frac{\partial \omega}{\partial k}, \qquad (7)$$

respectively. If $\frac{\omega}{k} \neq$ constant, each wavelet with different wave vector will have distinguished velocity. So the term $\omega = \omega(k)$ indicates a dispersion effect of the wave packet (Fig. 1b).

Particularly, the dispersion term of a surface wave in incompressible shallow fluid is given by

$$\omega(k) = \sqrt{gh}k - \frac{1}{6}\sqrt{gh}h^2 k^3, \qquad (8)$$

where h is the fluid depth, g is the gravitational acceleration (Belashov and Vladimirov, 2005).

In the complex space, we have $\frac{\partial}{\partial t} \leftrightarrow -i\omega$, and $\frac{\partial}{\partial x} \leftrightarrow ik$. Substituting into to Eq. (8), we obtain

$$\frac{\partial u}{\partial t} + \left(\sqrt{gh} + u\right)\frac{\partial u}{\partial x} + \frac{1}{6}\sqrt{gh}h^2\frac{\partial^3 u}{\partial x^3} = 0. \qquad (9)$$

Set $u' = u + \sqrt{gh}$, and $\beta = \frac{1}{6}\sqrt{gh}h^2$, then the equation is given by

$$\frac{\partial u'}{\partial t} + u'\frac{\partial u'}{\partial x} + \beta\frac{\partial^3 u'}{\partial x^3} = 0. \qquad (10)$$

This equation (similar to Eq. (1)) is one of the simplest forms of the KdV equation, balanced by both the nonlinear term $u\frac{\partial u}{\partial x}$ and dispersion term $\frac{\partial^3 u}{\partial x^3}$. Hereby the solution satisfying this equation will undergo no convergence or dispersion effect, and the wave shape could be maintained for a long time.

2.2 The solution of KdV equation and numerical simulation

Travelling wave could be represented by the form $u(x, t) = f(x - ct)$, where $u(x, t)$ represents a disturbance moving in the negative or positive x direction if $c < 0$ or $c > 0$, respectively [*Wazwaz*, 2009](Wazwaz, 2009). If the solution $u(x, t)$ depends only on the difference between the two coordinates of the partial differential equations, then the solution keeps its exact shape, and therefore called solitary waves. So a solitary wave is a travelling wave whose transition from the asymptotic state at $\xi = -\infty$ to the other asymptotic state at $\xi = \infty$ is localized in ξ, where $\xi = x - ct$, and c is the wave speed (Wazwaz, 2009).

Equation (10) or (1) has a special solution given by

$$u(x, t) = u_2 + (u_1 - u_2)\text{sech}^2\sqrt{\frac{u_1 - u_2}{12\beta}}(x - ct), \qquad (11)$$

where u_1 and u_2 are exhibited by Fig. 2a, and sech is referred to the hyperbolic secant function (Zabusky and Kruskal, 1965). This is just the bow wave observed by Russell in the early years, e.g. a solitary wave (Zabusky and Kruskal, 1965). Then u_2 represents the limiting wave amplitude of Eq. (11) at infinity, and u_1 characterizes the peak of the wave. Set $a = u_1 - u_2$ and

5 $d = \sqrt{12\beta/a}$, thus a is the amplitude and d is the width of the wave (shown by the vertical distance between the two red dashes of Fig. 2a). Figure 1a could possibly corroborate some descriptions of solitary wave properties as: (1) This wave propagates along x direction, e.g. with the form of $u(x - ct)$; (2) This wave is distributed in a limited space, e.g. $\lim_{x \to \pm\infty} u \to 0$; (3) The shape of the wave does not change with time. This specific kind of nonlinear wave is therefore called a soliton.

3 Observation results and discussions

10 The observational data from the Andes lidar from August 20, 2014 to July 7, 2019 are processed in detail as follows: (1) Select the typical Na_S event with intensity factor >3, and determine the Gaussian distribution function of the background sodium density profile on that day. (2) Subtract the Gaussian distribution from the original peak density profile of the Na_S. The net anomaly peak is obtained and next fitted by the soliton solution from the standard KdV equation. Find out the net anomaly distribution function and evaluate the quality of the fitting. (3) Compare evolutions of the net anomaly with the

15 solution of a generalized five-order KdV equation. Make a video to illustrate their variation processes, and intercept single-frames for this comparison.

3.1 The Gaussian distribution of the sodium density profile

It is shown that the sodium density variation with height can be approximated by the Gaussian distribution,

$$n_s(z) = \frac{C_s}{\sqrt{2\pi}\sigma_s} \exp[-\frac{(z - z_s)^2}{2\sigma_s^2}], \qquad (12)$$

20 where $n_s(z)$ is the sodium number density at z, C_s is the total column density of the sodium layer, z_s is the centroid height, and σ_s^2 is the RMS width (Xue, 2007).

When the Na_S occur, the sodium density suddenly increases in a narrow altitude and the density profile obviously deviates from the Gaussian distribution. To quantitatively explore this anomaly, the Gaussian distribution function of the background sodium density should be determined first.

25 The sodium density data observed at one night by the lidar compose of a two-dimensional matrix: the elements on the column vectors of the matrix represent the sodium densities at different heights at a given moment, and the elements on the row vectors represent the results at different moments at a given height. Now we choose the column vector of the matrix for data processing.

Set the origin observation data matrix of the day to be $\overleftrightarrow{\mathbf{M}}$, then $\overleftrightarrow{\mathbf{M}}$ is represented by the column vector as

$$\overleftrightarrow{\mathbf{M}} = [\overrightarrow{m}_1, \overrightarrow{m}_2, \dots, \overrightarrow{m}_{n-1}, \overrightarrow{m}_n], \qquad (13)$$

where n is the number of observational points on the day. Mark the maximum element in $\overleftrightarrow{\mathbf{M}}$ as d_{max}. If we select an Na_S event with intensity factor > 3, the critical value d_c for determining the anomalies is defined as

$$d_c = \frac{d_{max}}{3}, \qquad (14)$$

when the value of an element in the column vector is greater than d_c, it reflects the anomaly of Na density. Otherwise, it is considered that the column vector conforms to the Gaussian distribution of Na density on that day. The column vector reflecting the Na density anomaly is arranged into a matrix in the order of the observed time as

$$\overleftrightarrow{\mathbf{A}} = [\overrightarrow{a}_1, \overrightarrow{a}_2, \dots, \overrightarrow{a}_{k-1}, \overrightarrow{a}_k]. \qquad (15)$$

And then set the matrix of column vectors matching the Gaussian distribution in the order of observational moments to be

$$\overleftrightarrow{\mathbf{G}} = [\overrightarrow{g}_1, \overrightarrow{g}_2, \dots, \overrightarrow{g}_{n-k-1}, \overrightarrow{g}_{n-k}] \qquad (16)$$

To obtain the Gaussian distribution of Na density on that day, we average all column vectors in $\overleftrightarrow{\mathbf{G}}$ with a mark of $\overrightarrow{g}_{ave}$:

$$\overrightarrow{g}_{ave} = \frac{\sum_{i=1}^{n-k} \overrightarrow{g}_i}{n-k}, \qquad (17)$$

where $\overrightarrow{g}_{ave}$ reflects the distribution of Na density at altitude. As mentioned above, it is considered that $\overrightarrow{g}_{ave}$ is consistent with the Gaussian distribution, i.e., the result of a Gaussian fit with $\overrightarrow{g}_{ave}$ to the altitude h should satisfy Eq. (12).

Taking the Na_S observed on November 3, 2016 for example, the Gaussian fitting is made with the column vector $\overrightarrow{g}_{ave}$ and $\overrightarrow{h}$ according to Eq. (12). The fitting results are as follows

$$\overrightarrow{g}_h = 4330 \exp[-\frac{(\overrightarrow{h} - 92.86)^2}{7.798}], \qquad (18)$$

where $\overrightarrow{g}_h$ represents the modeled value that corresponds to the Gaussian distribution. The fitting result is shown as the red curve in Fig. 2c.

3.2 The net anomaly of sodium density and solitary wave fitting

Based on the observational data at Andes station from 20 August 2014 to 7 July 2019, 27 Na_S events are distinguished among 147 observation days. Continue to take the case on November 3, 2016 as an example. The column vector of d_{max} is denoted as $\overrightarrow{a}_d$ ($1 \le d \le k$). The profile of $\overrightarrow{a}_d$ with $\overrightarrow{h}$ is shown as the blue dash-dot line in Fig. 2c. The observed Na density can be regarded as the sum of Gaussian distribution and the anomaly. Thus, the vector $\overrightarrow{p}$ reflecting the net anomaly of Na density is given by the following equation

$$\overrightarrow{p} = \overrightarrow{a}_d - \overrightarrow{g}_h, \qquad (19)$$

and the distribution of $\overrightarrow{p}$ with $\overrightarrow{h}$ is shown as the blue dotted line in Fig. 2d. Then the peak density of $|\overrightarrow{p}|$ equals to 10180.95 cm^{-3}, with $|\overrightarrow{p}|$ to about zero at infinity.

Then the solitary wave fitting is performed on the vector $\vec{p}$. Since $\vec{p}$ reflects the net anomaly at a determined time (the moment of the peak density profile), the parameter t in the fitted formula is a constant. At this time the traveling wave $\xi = x - ct$ represents a specific phase. In order to better represent the altitude corresponding to the peak Na density, Eq. (11) could be written as

$$u(\xi) = u_2 + (u_1 - u_2)\text{sech}^2 \sqrt{\frac{u_1 - u_2}{12\beta}}(\xi - \xi_0), \tag{20}$$

where ξ_0 is the altitude corresponding to the maximum amplitude of the solitary wave. The fitting expression is finally deduced as

$$u(\xi) = -82.17 + 10263.12 * \text{sech}^2 \sqrt{\frac{10263.12}{19494.36}}(\xi - 93.63), \tag{21}$$

which means

$$u_2 = -82.17,$$
$$u_1 - u_2 = 10263.12 \text{ (or } u_1 = 10180.95),$$
$$12\beta = 19494.36,$$
$$\text{and}$$
$$\xi_0 = 93.63.$$

The fitting results are shown as the red curve in Fig. 2d. Now we know u_1 represents the peak density of the modeled curve, and u_2 corresponds to the density at infinity, i.e.

$$u(\xi) \underset{\xi \leq 80}{\approx} u(\xi) \underset{\xi \geq 110}{\approx} \lim_{\xi \to \infty} u(\xi) \to 0 \tag{22}$$

Let

$$\xi_1 = \pm\frac{d}{2} = \pm\sqrt{\frac{3\beta}{a}} = \pm\sqrt{3\beta/(u_1 - u_2)}, \tag{23}$$

putting it to Eq. (21), we have

$$u(\xi_1) = u_2 + \frac{4e}{(e+1)^2}(u_1 - u_2) = u(\pm 0.6891) = 8071.41, \tag{24}$$

which means the density at 0.6891 km from the peak is predicted to be 8071.41 (cm^{-3}). From Fig. 2d, we can find all these simulated values, u_1, u_2 and $u(\xi_1)$ are close to the observed results.

Furthermore, the theoretical full width at half maximum (FWHM) of a solution is given as:

$$h_{d/2} = \xi_0 + \frac{d}{2} = \xi_0 + \frac{\sqrt{\frac{12\beta}{u_1 - u_2}}}{2} \; (km). \tag{25}$$

To test the fitting results, the observed altitude of the selected case needs to be close to the calculated $h_{0.5}$. Since the vertical resolution of the lidar is limited to 0.5 km, we can perform linear interpolation for the observed altitude series. The interpolated vector $\vec{p}$ is denoted as $\vec{p_1}$, and the altitude series of $\vec{p_1}$ is marked as $\vec{h_1}$. The Na density at half width is $u(h_{d/2})$, then it is always possible to find a value closest to $u(h_{d/2})$ on both sides of the peak of $\vec{p_1}$ (denoted as $p_1(m)$ and $p_1(n)$).

The corresponding altitudes for $p_1(m)$ and $p_1(n)$ are noted as $h_1(m)$ and $h_1(n)$, respectively. Then the observed width of the soliton could be given as:

$$d' = h_1(n) - h_1(m). \tag{26}$$

According to the definition of the soliton, d' is also written as follows:

$$d' = \sqrt{\frac{12\beta'}{\max(\overrightarrow{p_1}) - 0}}, \tag{27}$$

where $\max(\overrightarrow{p_1})$ is the peak of $\overrightarrow{p_1}$;

0 is the density at infinity;

and β' is the β value deduced from the observation. It is shown that

$$\beta' = \frac{{d'}^2 \max(\overrightarrow{p_1})}{12}. \tag{28}$$

The deduced values of $h_{d/2}, d, d', u(h_{d/2}), p_1, \beta$ and β', for each Na_S event, are listed in Table 1. The fitting parameters on November 3, 2016 are also exhibited on Fig. 2d. Then the results show the fitting parameters are close to the observed values.

On the other hand, the column vector obtained by Eq. (21) is denoted as $\vec{q}$, then $\vec{q}$ is the predicted value at altitude h. Then some parameters to evaluate the fitting quality are needed. The coefficient of determination ($|R^2| < 1$) essentially measures the residual sum. The root mean square (RMSE) is also called the fitting standard deviation of a regression. They are calculated, respectively, as

$$R^2 = 1 - \frac{\sum_{i=1}^{L}(q_i - p_i)^2}{\sum_{i=1}^{L}(p_i - \bar{p}_i)^2}, \tag{29}$$

and

$$RMSE = \sqrt{\frac{1}{L}\sum_{i=1}^{L}(q_i - p_i)^2}, \tag{30}$$

where L is the length of vector $\vec{p}$ or $\vec{q}$, i.e., the number of observed altitude points.

The denominator of Eq. (29) denotes the residuals obtained by predicting net anomaly vector $\vec{p}$, and the numerator represents the residuals predicted using the modeled vector $\vec{q}$. When $R^2 < 0$, it means that the residuals of the results predicted by the anomaly model are larger than those obtained from the mean value of the vector $\vec{p}$ reflecting the net anomaly, indicating a poor result. When $R^2 > 0$, the larger R^2 indicates that the residuals are smaller, and the predicted effect is better.

The values of the parameters R^2 and RMSE obtained by fitting $\vec{p}$ and $\vec{q}$ for this Na_S event are calculated, respectively, as

$$R^2 = 0.9784,$$

and

$$RMSE = 315.8402,$$

showing a good fit with R^2 close to 1. Through the evaluation of fitting quality, it is confirmed that Eq. (23) can fit the net anomaly vector $\vec{p}$ within an allowable error. The fitting results and quality evaluation parameters are obtained, with 24/27 events having $R^2 > 0.9$ as shown in table 1. Therefore, the fitting results indicate $u(\xi)$ are consistent with the net anomaly $|\vec{p}|$.

5

3.3 Further explanation of Na$_S$ by higher-order solitary wave equation

In Fig. 2d, it is shown that some small wavelets appear on both wings of the blue dotted line drawn from the net anomaly vector $\vec{p}$, which could not be explained by the standard solitary equation with the red fitting curve. These wavelets, however, have similar characteristics to the higher-order solitary wave with a waveform shown as Fig. 2b.

10   Kawahara and Takuji proposed to add a higher-order dispersion term to the KdV equation, which considers dissipation, instability and higher-order dispersion effect in medium (Kawahara and Takuji, 2007). This generalized KdV equation is written as

$$\frac{\partial u}{\partial t} + u\frac{\partial u}{\partial x} + \beta\frac{\partial^3 u}{\partial x^3} + \gamma\frac{\partial^5 u}{\partial x^5} = 0, \tag{31}$$

which is also called the Kawahara equation (Kawahara and Takuji, 2007).

15   The numerical simulation results show that the Kawahara equation has two types of solutions: in the case of $\gamma > 0$ and $\beta \leq 0$, a soliton is formed with monotonic asymptotics similar to the soliton shown in Fig. 2a; in the case of $\gamma > 0$ and $\beta > 0$, the two wings of the soliton will have oscillation characteristics [*Mamun and Shukla*, 2009] (Mamun and Shukla, 2009). Taking $\beta = 1$ and $\gamma = 10^{-4}$, i.e., the expression of equation (28) will be

$$\frac{\partial u}{\partial t} + u\frac{\partial u}{\partial x} + \frac{\partial^3 u}{\partial x^3} + 10^{-4}\frac{\partial^5 u}{\partial x^5} = 0, \tag{32}$$

20   whose solution at $t = 0.0016$ is shown as Fig. 1b.

Further, we can study the evolution of the waveform over time using the Fourier transform method. Let the initial conditions be $\beta = 0.0023, \gamma = 10^{-4}$, and $u(x, 0) = e^{-36x^2}$. Since the Kawahara equation contains two variables, x and t, the simulation results are denoted as a two-dimensional matrix $\overleftrightarrow{\mathbf{W}}$. Then arrange $\overleftrightarrow{\mathbf{W}}$ by column vectors as follows

$$\overleftrightarrow{\mathbf{W}} = [\vec{w}_1, \vec{w}_2, \ldots, \vec{w}_{n-1}, \vec{w}_n]. \tag{33}$$

25   Since the vertical scale of the Na$_S$ is defined less than 10 km, while the horizontal scale is often reported more than 300 km or even over 1000 km (Fan et al., 2007; Ma et al., 2019), this scenario is in consistent with the shallow water model. The solitary waves could Particularly appear at the interface between upper and lower stratifications in the fluid medium [*Bogucki and Garrett*, 1993](Bogucki and Garrett, 1993). They are frequently found in the stratified or sheared places in the ocean and atmosphere (Doviak et al., 1991; Gan and Ingram, 1992; Huthnance, 1989). Therefore, it is more effective to look

30   for observational results related to stable stratifications or shears. The Na$_S$ event on April 9, 2019 is selected as an example (Fig. 3a). This Na$_S$ appears before the beginning of the observation at about 95 km altitude, with a downward propagation.

Atmospheric
Chemistry
and Physics
Discussions

The deduced vertical wind confirms the Na$_S$ occurs in downward vertical wind (shown as the negative value region in Fig. 3b). Figure 3c – e represent the zonal wind, meridional wind, and the temperature profiles, respectively. These three profiles indicate the Na$_S$ locating near the stratification with strong shear. Further, the stability of the stratification is determined by the Richardson number (Ri) (Liu, 2011; Nappo, 2002). Under stable stratification, both convection and turbulence are less likely to develop.

In unit time, due to vertical displacement, for a unit mass of air the convective flow energy to resist the net Archimedes buoyancy is

$$W_1 = -\overline{\frac{d}{dt}\left(\frac{1}{2}w^2\right)} = K_H N^2, \tag{34}$$

where

$w = dz/dt$, the vertical speed;

$K_H = \overline{wz} > 0$, the convective conductivity coefficient;

$N^2 = \frac{g}{T}\left(\frac{\partial T}{\partial z} + \frac{g}{C_p}\right)$, the buoyancy frequency;

$g = 9.5\ ms^{-2}$, the gravitational acceleration in the mesopause;

$C_p = 1004\ JK^{-1}kg^{-1}$, the specific heat at constant pressure;

and T is the atmospheric thermodynamic temperature.

On the other hand, for unit mass of air, the horizontal kinetic energy consumed per unit time in the presence of vertical wind shear, i.e., the kinetic energy provided to convective motion, is

$$W_2 = -\overline{\frac{d}{dt}\left(\frac{1}{2}\vec{V}_h^2\right)} = K_M\left[\left(\frac{\partial u}{\partial z}\right)^2 + \left(\frac{\partial v}{\partial z}\right)^2\right], \tag{35}$$

where u and v are the zonal and meridional wind velocities, respectively. $K_M > 0$ is the momentum transport coefficient and is usually approximately equal to K_H.

Thus, the stability of the layer depends on the value of W_1/W_2. When W_2 is less than W_1, it means that the disturbance kinetic energy converted by the basic airflow is less than the disturbance kinetic energy consumed by the stable stratification. In this situation, even if convection or turbulence occurs, it will be suppressed or weakened, so the atmosphere is in a stable state. The dimensionless ratio, W_1/W_2, is defined as

$$Ri = \frac{W_1}{W_2} = \frac{\frac{g}{T}\left(\frac{\partial T}{\partial z} + \frac{g}{C_p}\right)}{\left[\left(\frac{\partial u}{\partial z}\right)^2 + \left(\frac{\partial v}{\partial z}\right)^2\right]}, \tag{36}$$

which could be deduced from the wind and temperature results observed by the lidar (Fig. 3c – e). The calculated Ri with a value >1.5 are shown as black scatters in Fig. 3f. The Na$_S$ locates around the area where scatters are concentrated, i.e., a special stable area near 95 km. It is obvious that the Na$_S$ and stable region evolved synchronously, and finally both become blurred. Therefore, the lidar observations and deduced results are all consistent with the appearance of a solitary wave. A stable stratification with Ri >1.5 exists near about 95 km, accompanied by the zonal wind, meridional wind and temperature

being also stratified around 95 km. Once a fluctuation is excited in the vicinity of the stratification and just satisfies the balance of nonlinear and dispersion effects, the waveform will maintain through the propagation, i.e., a solitary wave appears.

Furthermore, the evolution of observed net anomaly for the Na_s throughout whole night is also needed for a comparison. In section 3.1, the initial observation of sodium density is denoted as

$$\overleftrightarrow{\mathbf{M}} = [\vec{m}_1, \vec{m}_2, ..., \vec{m}_{n-1}, \vec{m}_n].$$

Note the Gaussian distribution model of the current day as a two-dimensional matrix $\overleftrightarrow{\mathbf{G}}_0$, and define $\overleftrightarrow{\mathbf{G}}_0$ as isomorphic to $\overleftrightarrow{\mathbf{M}}$. Then $\overleftrightarrow{\mathbf{G}}_0$ could be written in the form of column vector as

$$\overleftrightarrow{\mathbf{G}}_0 = [\vec{g}_h, \vec{g}_h, ..., \vec{g}_h, \vec{g}_h]. \tag{37}$$

Obviously, the net anomaly evolution of the Na_S is obtained by observation data matrix $\overleftrightarrow{\mathbf{M}}$ subtracting the Gaussian distribution model $\overleftrightarrow{\mathbf{G}}_0$, which could be denoted as $\overleftrightarrow{\mathbf{S}}$. There are

$$\overleftrightarrow{\mathbf{S}} = \overleftrightarrow{\mathbf{M}} - \overleftrightarrow{\mathbf{G}}_0 = [\vec{m}_1 - \vec{g}_h, \vec{m}_2 - \vec{g}_h, ..., \vec{m}_{n-1} - \vec{g}_h, \vec{m}_n - \vec{g}_h]$$
$$= [\vec{s}_1, \vec{s}_2, ..., \vec{s}_{n-1}, \vec{s}_n], \tag{38}$$

where $\vec{s}_i (i = 1、2、...、n-1、n)$ is the column vector of $\overleftrightarrow{\mathbf{S}}$.

In order to compare the numerical simulation results $\overleftrightarrow{\mathbf{W}}$ with the Na_S evolution model $\overleftrightarrow{\mathbf{S}}$ more intuitively, the Fourier transform method is used uniformly to disperse a certain period of time on the time variable t into n moments in the numerical simulation. Thus, both $\overleftrightarrow{\mathbf{W}}$ and $\overleftrightarrow{\mathbf{S}}$ are two-dimensional matrices with the same column number n. To better show them, a dynamic video of the variation of their column vectors with time has been made (uploaded as Data Repository, https://dx.doi.org/10.12176/01.99.02129). The five left images in Fig. 4 (i.e., Fig. 3a, c, e, g, i) are single-frame intercepted from $\overleftrightarrow{\mathbf{W}}$ of the video, showing the evolutions of the five-order solitary wave over time. And the five images on the right (i.e., Fig. 4b, d, f, h, j) are intercepted from $\overleftrightarrow{\mathbf{S}}$, indicating variations of the net anomaly of the Na_S. Figure 4a and b show at this moment, the simulated wave shape are similar to the observed peak density profile. Figure 4c and d: the huge peaks attenuate gradually. Figure 4e and f: the peaks decay to about zero value. Figure 4g and h: the peaks change phase and resume. Figure 4i and j: the peaks recover to a sharp form similar to the initial condition, except with different phase. By comparison, it is verified that the numerical simulation results $\overleftrightarrow{\mathbf{W}}$ are in good agreement with the evolution process $\overleftrightarrow{\mathbf{S}}$ of the Na_S. So the five-order solitary wave theory is appropriate in explaining this Na_S event.

However, it is worth noting that the numerical simulation of the higher-order KdV equation is probably only suitable for explaining the events similar to the selected case. These events are typically characterized by occurrence heights below 95 km, longer durations, and descending patterns similar to tidal fluctuations. In contrast, the other events with shorter durations and cloud-like shapes are less consistent with the higher-order simulation results. This discrepancy also implies that the Na_S with different characteristics may have different fine structures.

Atmospheric
Chemistry
and Physics
Discussions

4 Conclusions

In this research, the solitary wave theory is applied to study the Na_S. Among the observations of Andes lidar from August 20, 2014 to July 7, 2019, 27 Na_S cases with intensity factor>3 have been selected for processing through the Gaussian and soliton fitting steps. The original observed peak density profile of the Na_S is subtracted by the Gaussian distribution, and then the net anomaly peak is obtained. The net peak is fitted by the soliton solution from the standard KdV equation, and the quality of the fitting is then evaluated. Statistical results reveal that in 24/27 cases, the net peak of Na_S exhibits similar features to a soliton. Time series of the net anomaly on 9 April, 2019 reveals a similar variation process to the solution of a five-order KdV equation. Although still highly uncertain, this solitary wave theory could possibly explain some characteristics of Na_S.

Data availability

The regular ALO Na Lidar data between 80 and 105 km is publicly available from the Andes Lidar Observatory database at http://lidar.erau.edu/data/nalidar/.

Author information

Affiliations

Department of Geophysics, College of the Geology Engineering and Geomatics, Chang'an University, Xi'an, 710054, China

Shican Qiu, Mengxi Shi, & Peng Ju

Key Laboratory of Geospace Environment, Chinese Academy of Sciences, University of Science & Technology of China, Hefei, Anhui, 230026

Shican Qiu, Xianghui Xue, Tao li & Xiankang Dou

Center for Environmental Research and Earth Sciences (CERES), Salem, MA 01970, USA

Willie Soon

Institute of Earth Physics and Space Science (ELKH EPSS), 9400, Sopron, Hungary

Willie Soon

Shandong Guoyao Quantum Lidar Co., Ltd., Jinan, 250101, China

Atmospheric
Chemistry
and Physics
Discussions

Mingjiao Jia

Mengcheng National Geophysical Observatory, School of Earth and Space Sciences, University of Science and Technology of China, Hefei, Anhui, 230026, China

5   Xianghui Xue, Tao li & Xiankang Dou

Contributions

Shican Qiu conceived this study and wrote this manuscript.

Mengxi Shi performed data analysis and prepared Fig. 1 and Fig. 3.

10   Willie Soon was in charge of the organization and English polishing of the whole manuscript.

Mingjiao Jia prepared Fig. 2 and gave some useful comments on the content.

Xianghui Xue wrote the response to reviewers and added some materials in the discussion.

Tao Li helped with the response to reviewers.

Peng Ju helped discuss with the KdV equations.

15   Xiankang Dou conceived this study and provided data from the Chinese Meridian Project.

Competing interests

The authors declare no conflict of interest.

20

References

Ban, C., Li, T., Xiong, J., Dou, X., and Fang, X.: Sodium lidar–observed gravity wave breaking followed by an upward propagation of sporadic sodium layer over Hefei, China, Journal of Geophysical Research A Space Physics 120, doi:10.1002/2015JA021339, 2015.

25   Belashov, V. Y., and Vladimirov, S. V.: Solitary Waves in Dispersive Complex Media, Springer Series in Solid-State Sciences, Springer, Berlin, Heidelberg, XIV, 294 pp., 2005.

Benci, V., and Fortunato, D.: Variational Methods in Nonlinear Field Equations, Springer Monographs in Mathematics, Springer, Cham, Switzerland, XIX, 253 pp., 2014.

Bogucki, D., and Garrett, C.: A Simple Model for the Shear-induced Decay of an Internal Solitary Wave, Journal of Physical

30   Oceanography, 23, 1767–1776, 10.1175/1520–0485(1993)0232.0.CO;2, 1993.

Chen, L., and Yi, F.: Average properties and small-scale variations of the mesospheric Na and Fe layers as observed simultaneously by two closely colocated lidars at 30° N, Annales Geophysicae, 29, 1037–1048, 2011.

Clemesha, B. R., Kirchhoff, V. W. J. H., Simonich, D. M., and Takahashi, H.: Evidence of an extra-terrestrial source for the mesospheric sodium layer, Geophysical Research Letters, 5, 873–876, 1978.

Clemesha, B. R., Batista, P. P., and Simonich, D. M.: Wave–Associated Sporadic Neutral Layers in the Upper Atmosphere, 5th International Congress of the Brazilian Geophysical Society, 15, 10.1590/S0102–261X1997000300003, 1997.

5 Collins, S. C., Plane, J. M. C., Kelleya, M. C., Wright, T. G., Soldán, P., Kanee, T. J., Gerrarde, A. J., Grime, B. W., Rollason, R. J., and Friedman, J. S.: A study of the role of ion–molecule chemistry in the formation of sporadic sodium layers, Journal of Atmospheric & Solar Terrestrial Physics, 64, 845–860, 2002.

Cox, R. M., Plane, J. M. C., and Green, J. S. A.: A modelling investigation of sudden sodium layers, Geophysical Research Letters, 20, 2841–2844, 1993.

10 Cox, R. M., and Plane, J. M. C.: An ion-molecule mechanism for the formation of neutral sporadic Na layers, Journal of Geophysical Research Atmospheres, 103, 6349–6359, 1998.

Dou, X. K., Xue, X. H., Chen, T. D., Wan, W. X., and Chen, Z. Y.: A statistical study of sporadic sodium layer observed by Sodium lidar at Hefei (31.8° N, 117.3° E), Annales Geophysicae, 27, 2247–2257, 2009.

Dou, X. K., Xue, X. H., Li, T., Chen, T. D., Chen, C., and Qiu, S. C.: Possible relations between meteors, enhanced electron

15 density layers, and sporadic sodium layers, Journal of Geophysical Research: Space Physics, 115, A06311, 2010.

Doviak, R. J., Chen, S. S., and Christie, D. R.: A Thunderstorm–Generated Solitary Wave Observation Compared with Theory for Nonlinear Waves in a Sheared Atmosphere, Journal of the Atmospheric Sciences, 48, 87–111, 1991.

Fan, Z. Y., Plane, J. M. C., and Gumbel, J.: On the global distribution of sporadic sodium layers, Geophysical Research Letters, 34, 87-101, 2007.

20 Gan, J., and Ingram, R. G.: Internal hydraulics, solitons and associated mixing in a stratified sound, JOURNAL OF GEOPHYSICAL RESEARCH, 97, 9669–9688, 10.1029/92JC00491, 1992.

Gardner, C. S., and Voelz, D. G.: Lidar studies of the nighttime sodium layer over Urbana, Illinois: 2. Gravity waves, Journal of Geophysical Research Space Physics, 92, 4673–4694, 1987.

Gardner, C. S., Kane, T. J., Senft, D. C., Qian, J., and Papen, G. C.: Simultaneous observations of sporadic E, Na, Fe, and

25 Ca^+ layers at Urbana, Illinois: Three case studies, Journal of Geophysical Research: Atmospheres, 98, 16865–16873, 1993.

Gardner, C. S., Guo, Y., and Liu, A. Z.: Parameterizing Wave-Driven Vertical Constituent Transport in the Upper Atmosphere, Earth & Space Science, 6, 904–913, 2019.

Gong, S., Yang, G., Cheng, X. W., Gong, S., Xu, J., Li, F., Wei, G., and Wang, J. H.: Lidar observation campaigns on

30 diurnal variations of the sodium layer in Beijing and Wuhan, China, ence China Earth ence, 58, 1377–1386, 2015.

Hansen, G., and von Zahn, U.: Sudden sodium layers in polar latitudes, Journal of Atmospheric & Solar Terrestrial Physics, 52, 585–608, 1990.

Heinrich, D., Nesse, H., Blum, U., Acott, P., Williams, B., and Hoppe, U. P.: Summer sudden Na number density enhancements measured with the ALOMAR Weber Na Lidar, Annales Geophysicae, 26, 1057–1069, 2008.

Heinselman, C. J., Thayer, J. P., and Watkins, B. J.: A high–latitude observation of sporadic sodium and sporadic E-layer formation, Geophysical Research Letters, 25, 3059–3062, 1998.

Huthnance, J. M.: Internal tides and waves near the continental shelf edge, Geophys. Astrophys. Fluid Dyn., 48, 81–106, 1989.

5 Kane, T. J., Hostetler, C. A., and Gardner, C. S.: Horizontal and vertical structure of the major sporadic sodium layer events observed during ALOHA–90, Geophysical Research Letters, 18, 1365–1368, 1991.

Kane, T. J., and Gardner, C. S.: Lidar Observations of the Meteoric Deposition of Mesospheric Metals, ence, 259, 1297–1300, 1993.

Kawahara, and Takuji: Oscillatory Solitary Waves in Dispersive Media, Journal of the Physical Society of Japan, 33, 260–264, 10.1143/JPSJ.33.260, 2007.

10

Kirkwood, S., and Nilsson, H.: High–latitude Sporadic–E and other Thin Layers – the Role of Magnetospheric Electric Fields, Space ence Reviews, 91, 579–613, 2000.

Kopp, E.: On the abundance of metal ions in the lower ionosphere, Journal of Geophysical Research Space Physics, 102, 9667–9674, 1997.

15 Korteweg, D. J., and Vries, G. D.: On the change of form of long waves advancing in a rectangular canal, and on a new type of long stationary waves, Philosophical Magazine, 39(240), 422–443, 1895.

Li, T., She, C. Y., Liu, H. L., Leblanc, T., and Mcdermid, I. S.: Sodium lidar–observed strong inertia-gravity wave activities in the mesopause region over Fort Collins, Colorado (41°N, 105°W), Journal of Geophysical Research Atmospheres, 112, D22104, 2007a.

20 Li, T., She, C. Y., Liu, H. L., and Montgomery, M. T.: Evidence of a gravity wave breaking event and the estimation of the wave characteristics from sodium lidar observation over Fort Collins, CO (41°N, 105°W), Geophysical Research Letters, 34, L05815, 2007b.

Liu, A. Z., Guo, Y., Vargas, F., and Swenson, G. R.: Horizontal wind and temperature in the lower thermosphere (80–140 km) measured by a Na Lidar at Andes Lidar Observatory, Geophysical Research Letters, 43, 2374–2380, 10.1002/2016GL068461, 2016.

25

Liu, S. D., Liu, S.K.: Dynamics of the Atmosphere, 2 ed., the Publishing House of Beijing University, Beijing 2011.

Liu, Y., and Yi, F.: Behavior of sporadic Na layers on small time scale, Journal of Atmospheric and Solar–Terrestrial Physics, 71, 1374–1382, 2009.

Liu, Y. J., Clemesha, B. R., Wang, J. H., and Cheng, X. W.: Comparison of sporadic sodium layer characteristics observed at different time resolutions, Annales Geophysicae, 31, 1899–1912, 2013.

30

Ma, J., Xue, X., Dou, X., Chen, T., Tang, Y., Jia, M., Zou, Z., Li, T., Fang, X., and Cheng, X.: Large–Scale Horizontally Enhanced Sodium Layers Coobserved in the Midlatitude Region of China, Journal of Geophysical Research: Space Physics, 2019.

Mamun, A. A., and Shukla, P. K.: Effects of nonthermal distribution of electrons and polarity of net dust–charge number density on nonplanar dust–ion–acoustic solitary waves, Physical Review E 80, 037401, 10.1103/PhysRevE.80.037401, 2009.

Mathews, J. D., Zhou, Q., Philbrick, C. R., Morton, Y. T., and Gardner, C. S.: Observations of ion and sodium layer coupled processes during AIDA, Journal of Atmospheric & Terrestrial Physics, 55, 487–498, 1993.

Nagasawa, C., and Abo, M.: Lidar observations of a lot of sporadic sodium layers in mid–latitude, Geophysical Research Letters, 22, 263–266, 1995.

Nappo, C. J.: An introduction to atmospheric gravity waves, International Geophysics, 85, 1–216, 10.1016/b978–0–12–385223–6.00001–x, 2002.

Nesse, H., Heinrich, D., Williams, B., Hoppe, U. P., Stadsnes, J., Rietveld, M., Singer, W., Blum, U., Sandanger, M. I., and Trondsen, E.: A case study of a sporadic sodium layer observed by the ALOMAR Weber Na lidar, Annales Geophysicae, 26, 1071–1081, 2008.

Plane, J., Feng, W., and Dawkins, E.: The Mesosphere and Metals: Chemistry and Changes, Chemical Reviews, 115, 4497, 2015.

Plane, J. M. C.: Atmospheric chemistry of meteoric metals, Chemical Reviews, 103, 4963–4984, 2003.

Prasanth, P. V., Kumar, Y. B., and Rao, D. N.: Lidar observations of sporadic Na layers over Gadanki (13.5° N, 79.2° E), Annales Geophysicae, 25, 1759–1766, 10.5194/angeo–25–1759–2007, 2007.

Qian, J., Gu, Y., and Gardner, C. S.: Characteristics of the sporadic Na layers observed during the Airborne Lidar and Observations of Hawaiian Airglow/Airborne Noctilucent Cloud (ALOHA/ANLC–93) campaigns, Journal of Geophysical Research Atmospheres, 103, 6333–6347, 1998.

Qiu, S. C., Tang, Y., Jia, M., Xue, X., and Wang, Y.: A review of latitudinal characteristics of sporadic sodium layers, including new results from the Chinese Meridian Project, Earth–Science Reviews, 162, 83–106, 2016.

Qiu, S. C., N., W., Soon，W., Lu，G.P., and Dou, X. K.: Sporadic sodium layer: A possible tracer for the conjunction between the upper and lower atmospheres, 10.5194/acp–2020–1079, 2020.

Russell, J. M.: Report of the Fourteenth Meeting of the British Association for the Advancement of Science, London, 311–390, 1844.

V1. NSSDC Space Science Article Data Repository. https://dx.doi.org/10.12176/01.99.02129.

von Zahn, U., von der Gathen, P., and Hansen, G.: Forced Release of Sodium from Upper Atmospheric Dust Paaticles, Geophysical Research Letters, 14, 76–79, 1987.

von Zahn, U., and Hansen, T. L.: Sudden neutral sodium layers : a strong link to sporadic E layers, Journal of Atmospheric & Terrestrial Physics, 50, 93–104, 1988.

Wazwaz, A. M.: Partial Differential Equations and Solitary Waves Theory, Nonlinear Physical Science, Springer, Berlin, Heidelberg, 2009.

Williams, B. P., Croskey, C. L., She, C. Y., Mitchell, J. D., and Goldberg, R. A.: Sporadic sodium and E layers observed during the summer 2002 MaCWAVE/MIDAS rocket campaign, Annales Geophysicae, 24, 1257–1266, 2006.

Xu, J., and Smith, A. K.: Studies of gravity wave–induced fluctuations of the sodium layer using linear and nonlinear models, Journal of Geophysical Research Atmospheres, 109, D02306, 2004.

5 Xue, X. H.: Studies on Geoeffectiveness of Coronal Mass Ejections and Near–Earth Space Environment, Ph.D, University of Science & Technology of China, Hefei, China, 2007.

Zabusky, N. J., and Kruskal, M.: Interaction of "Solitons" in a Collisionless Plasma and the Recurrence of Initial States, Physical Review Letters, 15, 240–243, 10.1103/PhysRevLett.15.240, 1965.

Zhou, Q., Mathews, J. D., and Tepley, C. A.: A proposed temperature dependent mechanism for the formation of sporadic

10 sodium layers, Journal of Atmospheric & Terrestrial Physics, 55, 513–521, 1993.

Zhou, Q., and Mathews, J. D.: Generation of sporadic sodium layers via turbulent heating of the atmosphere?, Journal of Atmospheric & Terrestrial Physics, 57, 1309–1315, 1995.
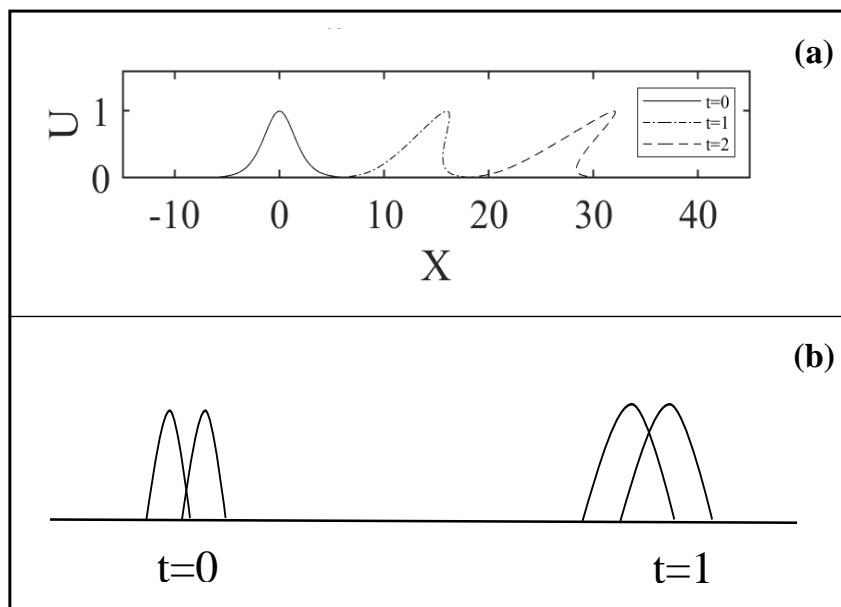
Figure 1: The convergence (a) and dispersion (b) effects of a wave. (a) The wave packet front becomes steeper and steeper as the wave propagates, leading to a nonlinear effect of convergence. (b) The dispersion effect for the wave packet.
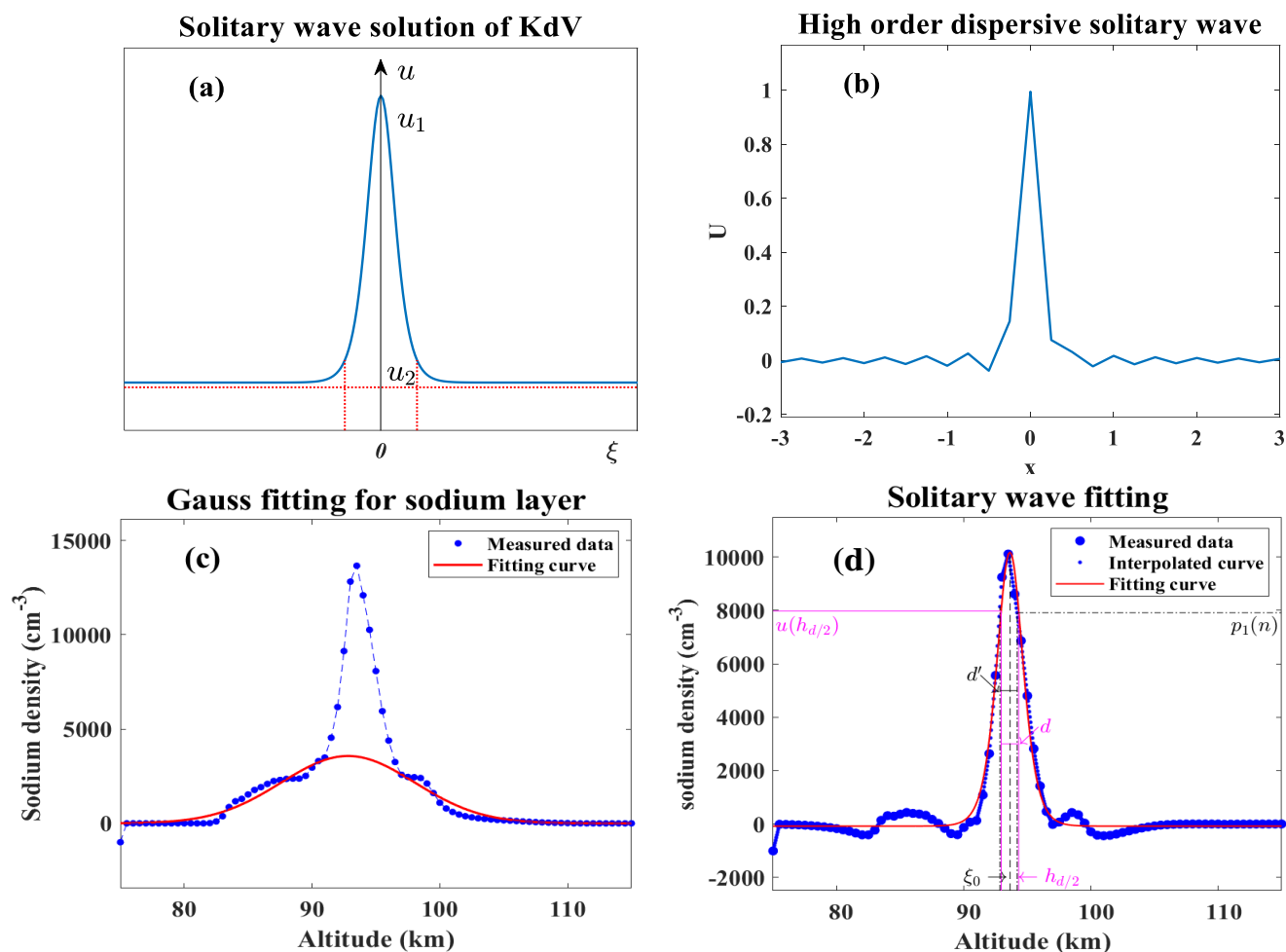
Figure 2: Comparison of the theoretical solitary wave profiles and observed peak density profiles of NaS. (a) The solitary wave profile according to Eq. (11), with u_2 representing the limiting wave amplitude at infinity and u_1 characterizing the peak of the wave. The width $d = \sqrt{12\beta/a}$ is determined by the vertical distance between the two red dashes. (b) Simulated solution of the five-order solitary wave. (c) The peak density profile of the NaS. The blue dash-dot line represents the peak sodium density observed on November 03, 2016. The red curve indicates fitted background Gaussian distribution throughout the whole night. (d) The fitting image of the peak profile. The blue dotted line shows the distribution of the observed data after subtracting the background Gaussian distribution from 2c, while the red curve is simulated according to Eq. (11) with appropriate parameters. The blue dotted line is very close to the red curve, except some wing features similar to 2b. The fitting parameters of $h_{d/2}, d, d', u(h_{d/2})$ and $p_1(n)$ are also given.
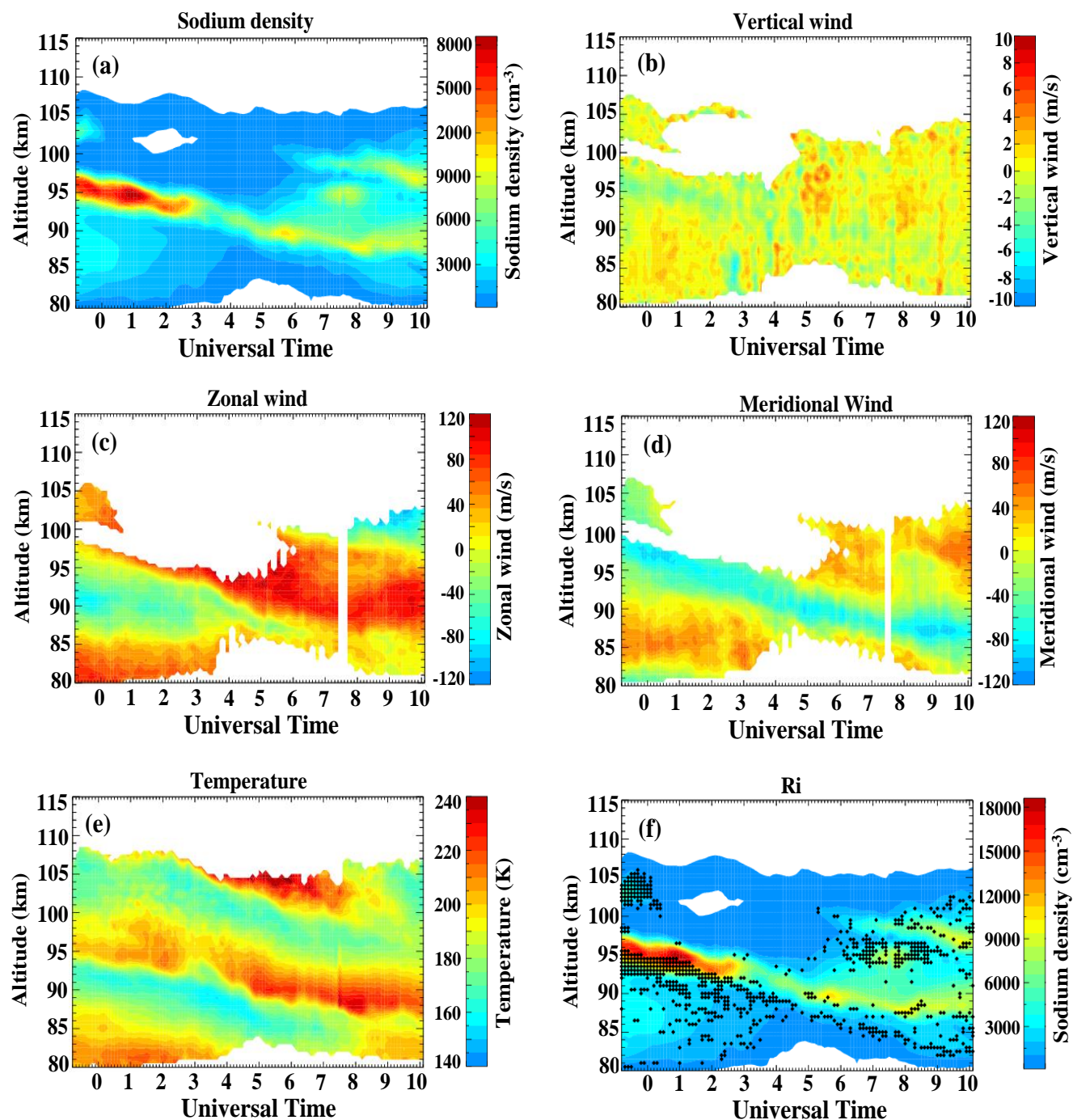
Figure 3: Observations and results from the Andes lidar on April 9, 2019. The empty areas indicate a low signal-to-noise ratio (SNR) and large error of the observed data. (a) The sodium density profile. The Nas appears before the beginning of the observation, at about 95 km altitude. (b) The vertical wind observations. (c) The zonal wind profile. (d) The meridional wind profile. (e) The temperature variations. (f) The calculated Ri distributions. The black scatter dots represent Ri with a value >1.5.
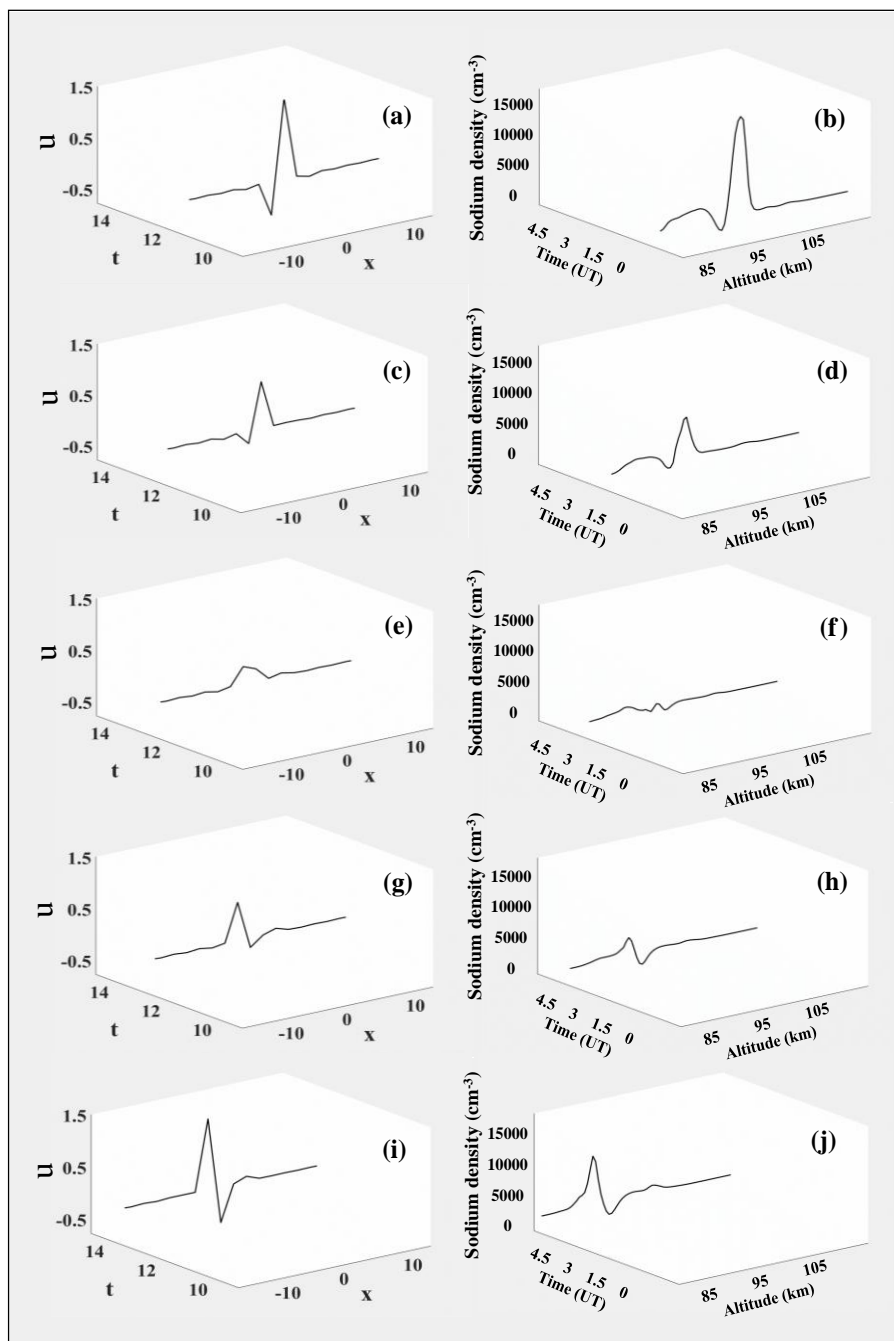
Figure 4: Comparison of five-order solitary wave evolution images over time and Na density net anomalies observed at the Andes station on April 9, 2019. (a) and (b): at this moment, the simulated wave shape is similar to the observed peak density profile. (c) and (d): the huge peaks attenuate synchronously. (e) and (f): the peaks decay to about zero value. g and h: the peaks change phase and resume. (i) and (j): the peaks recover to a sharp form similar to the initial condition, except with different phase. A dynamic video of the variation of their column vectors with time has been made and uploaded as DOI:10.12176/01.99.02129.

5

Table 1. Statistics of fitting parameters and fitting quality evaluation for the observations at Andes station from August 20, 2014 to July 7, 2019

Parameter / Event	Parameter of Solitary Equation						Parameter of Solitary Wave Width					
	u_1 (cm^{-3})	u_2 (cm^{-3})	β (m^{-1}) $\times 10^{12}$	ξ_0 (km)	RMSE	R^2	$h_{d/2}$ (km)	d (km)	d' (km)	$u(h_{d/2})$ (cm^{-3})	$p_1(n)$ (cm^{-3})	β' (m^{-1}) $\times 10^{12}$
2014-08-20	12441.3	-102.3	877.0	90.46	462.0	0.9612	90.92	0.92	0.85	9761.5	9723.6	763.3
2015-01-30	21676.5	-185.9	5938.7	94.06	625.9	0.9867	94.96	1.81	2	16982.8	16965.3	6997.9
2015-02-02	42591.4	638.8	6625.1	94.56	2226.9	0.945	95.25	1.38	1.3	33585.2	33714.0	6100.0
2015-04-18	14265.7	-221.2	6860.8	98.03	1462.5	0.8814	99.22	2.38	1.45	11170.3	11090.7	2624.0
2015-04-19	12100.9	-294.4	10571.7	89.2	1151.0	0.9152	90.80	3.20	2.8	9460.0	9425.1	9028.6
2015-04-21	10863.3	-699.4	4055.2	91.58	643.8	0.9561	92.61	2.05	2	8381.8	8423.7	3547.1
2015-04-22	15853.3	494.6	3668.7	88.95	894.3	0.9445	89.80	1.69	1.55	12564.1	12637.9	3406.4
2015-11-06	12555.5	16.5	755.3	92.55	532.6	0.9457	92.98	0.85	0.85	9857.4	9803.9	731.7
2016-02-25	5602.8	158.2	1312.0	91.99	277.0	0.9573	92.84	1.70	1.7	4451.5	4445.6	1329.6
2016-03-02	7023.3	107.5	378.2	92.96	238.1	0.962	93.37	0.81	0.7	5565.7	5536.8	294.7
2016-03-15	6590.4	325.7	2703.1	94.94	491.5	0.9224	96.08	2.28	2.3	5255.4	5260.4	2980.0
2016-06-06	10644.9	586.4	2464.4	91.23	634.5	0.9362	92.09	1.71	1.75	8498.7	8426.6	2876.3
2016-10-26	16359.1	-252.6	1197.3	96.88	1076.1	0.8772	97.35	0.93	0.85	12863.6	12744.1	962.2
2016-10-28	7372.1	12.1	776.0	97.33	412.2	0.9192	97.89	1.12	1.1	5796.4	5810.6	720.3
2016-11-03	10181.0	-82.2	1624.5	93.63	315.8	0.9784	94.32	1.38	1.35	7979.4	7914.6	1536.4
2016-11-09	12595.5	82.1	753.6	92.8	620.9	0.9181	93.23	0.85	0.8	9966.6	9880.7	638.1
2017-04-22	31064.8	-424.9	3944.1	96.29	1298.5	0.9578	96.90	1.23	1.25	24363.0	24502.0	4016.3
2017-11-25	9205.2	-31.2	699.7	94.79	256.4	0.9784	95.27	0.95	0.9	7245.7	7158.5	600.1
2017-11-28	8995.4	-8.7	974.1	97.05	454.1	0.9416	97.62	1.14	1.15	7085.2	7066.9	978.4
2017-12-16	11306.7	193.5	2482.5	96.48	656.9	0.9414	97.30	1.64	1.5	8928.1	8945.1	2249.8
2017-12-17	7019.4	1.6	828.7	92.64	159.1	0.9881	93.24	1.19	1.2	5526.0	5525.2	814.2
2017-12-19	12824.9	-68.1	1388.5	96.1	493.6	0.9654	96.67	1.14	5.8	2977.6	2995.4	18319.9
2017-12-21	4522.8	-20.5	4225.3	94.44	786.3	0.7611	96.11	3.34	2.95	5423.3	5435.3	5842.3
2017-12-22	7491.7	-61.9	3933.2	94.66	696.0	0.9024	95.91	2.50	1.3	8190.9	8208.6	2131.7
2019-04-07	17210.2	66.4	641.5	95.29	403.8	0.9784	95.63	0.67	1.9	13379.5	13314.1	5090.4
2019-04-09	18618.4	488.4	2708.2	94.82	1178.4	0.9179	95.49	1.34	1.45	14755.6	14738.4	2964.7
2019-07-06	12787.4	-256.7	3345.4	92.97	546.2	0.9714	93.85	1.75	1.65	10020.7	9985.5	2934.3